Time Domain Analysis of Graphene Nanoribbon Interconnects Based on Transmission Line Model

S. Haji Nasiri[*], M. K. Moravvej-Farshi[**] and R. Faez[***]

Time domain analysis of multilayer graphene nanoribbon (MLGNR) interconnects, based on transmission line modeling (TLM) using a six-order linear parametric expression, has been presented for the first time. We have studied the effects of interconnect geometry along with its contact resistance on its step response and Nyquist stability. It is shown that by increasing interconnects dimensions their propagation delays are increased and accordingly the system becomes relatively more stable. In addition, we have compared time responses and Nyquist stabilities of MLGNR and SWCNT bundle interconnects, with the same external dimensions. The results show that under the same conditions, the propagation delays for MLGNR interconnects are smaller than those of SWCNT bundle interconnects are. Hence, SWCNT bundle interconnects are relatively more stable than their MLGNR rivals.

Keywords: Graphene, Interconnects, Nanoribbon, Nyquist Stability, Time domain analysis.

1. Introduction

Recent developments in science and technology of graphene nanoribbons (GNRs) have stimulated up major interest in GNR potential applications, particularly as transistors and interconnects [1-3]. Since each GNR can be considered as an unrolled single wall carbon nanotube (SWCNT), most of GNR electronic properties are similar to those of SWCNT. Depending on its geometry, GNR can be either metallic or semiconducting [4-6]. In a high-quality sheet of graphene, carriers' mean free path (MFP) can be as long as λ=1 μm, the thermal conductivity can be as large as 3-5×10^3 W/mK, and it is capable of conducting current densities as high as 10^8 A/cm^2 [7]. Moreover, its electrical conductivity is a linearly increasing function of temperature beyond T=300 K [8, 9]. The major advantage of GNR over CNT is its more straightforward fabrication processes [10].

These extraordinary properties have made GNR a potential material for signal and power interconnects. Interconnects made of GNRs can potentially be used either as intra-cell interconnects linking GNR transistors in a seamless fashion [1, 3] or in a multilevel interconnect network as conventional interconnects [11]. The former interconnects reduce the number of metal-to-graphene connections resulting in elimination of some contact and quantum resistances, which in turn, improves the circuit performance. The latter interconnects; on the other hand, require more versatile growth approaches for graphene. This, in turn, can potentially reduce the propagation delays and power dissipations, so improving the system reliability.

While each GNR has desirable material properties, it suffers from an intrinsic ballistic (quantum) resistance that is independent of GNR′s length (l) and is approximated by $h/2e^2N_{ch}\approx 12.5/N_{ch}$ (KΩ), wherein h, e, and N_{ch} are the Planck′s constant, electron charge, and the number of conduction channels in a GNR, respectively [7]. Such a high intrinsic resistance that is length independent leads to excessive delay for interconnects applications. On the other hand, multilayer GNRs (MLGNRs) with reduced equivalent resistance have been physically demonstrated to be suitable media for local, intermediate, and global interconnects [10].

Most of the feasibility studies toward the use of GNRs as interconnects medium, in recent years, have been devoted to physical prospects [2, 6, 12-15], technological aspects [7, 10] and some physical-based circuit modeling of GNRs [10]. In spite of all these

Iranian Journal of Electrical & Electronic Engineering, 2012.
Paper first received 9 Dec. 2010 and in revised form 30 Nov. 2011.
[*] The Author is with the Department of Electrical Engineering, Science and Research Branch, Islamic Azad University, Tehran 1477893855, Iran.
E-mail: s.nasiri@qiau.ac.ir.
[**] The Author is with the School of Electrical and Computer Engineering, Advanced Device Simulation Lab (ADSL), Tarbiat Modares University, P. O. Box 14115-143, Tehran 1411713116, Iran (Corresponding Author).
E-mail: farshi_k@modares.ac.ir.
[***] The Author is with the Electrical Engineering Department, Sharif University of Technology, Tehran, Iran.
E-mail: faez@sharif.edu.

valuable research works, only one paper has focused on Nyquist stability analysis [16] and no efforts have been reported on time domain analysis of GNR interconnects, so far.

On the other hand performance of local (on-chip) interconnects are vital to the analog ICs designed for radio frequency (RF) applications [17]. In other words, possible high overshoots/undershoots in the time domain responses of on-chip interconnects used in an RF-IC can deteriorate the IC performance. In order to analyze the performance of MWCNT interconnects designed for such on-chip applications, we need to evaluate their time domain responses and stabilities.

Aim of this paper is to report the results of our studies on time domain analysis of the driver-MLGNR-load system, using a transmission line model (TLM). In this study, we have examined the effects of the MLGNR geometry and its contact resistance on interconnects time domain response and stability. Finally, numerical results for MLGNR were compared with those obtained for interconnect composed of single wall carbon nanotube (SWCNT) bundles of the same external dimensions.

2. Time Domain Response

Figure 1(a) illustrates a schematic representation of a typical RLC model for MLGNR interconnects made of N Parallel GNRs of the same lengths l and widths W. In this figure, R_C, R_Q, and R_S represent the equivalent resistances introduced by the imperfect contacts, the quantum effect, and the carriers' scatterings, respectively. The equivalent quantum resistance for this MLGNR equals that of each constituent GNR divided by N; i.e., $R_Q \approx 12.5/NN_{ch}$ (KΩ). When the length of each GNR is greater than its carriers′ mean free path (i.e., $l>\lambda$), the equivalent distributed ohmic resistance (per unit length), introduced by carriers scatterings with defects, substrate-induced disorders, and phonons, can be written as $R_S \equiv R_Q/\lambda \approx 12.5/\lambda NN_{ch}$ (KΩ-cm^{-1}) [10]. Also shown in Fig. 1(a) C_E (F-cm^{-1})$\approx \varepsilon W/d$ and $C_Q \approx \{R_Q v_F\}^{-1} = (NN_{ch}/1.25)$ pF-cm^{-1} are the per unit length values of the equivalent capacitances induced by the electrostatic and quantum effects, respectively, in which ε and v_F ($=10^8$ cm-s^{-1}) are the dielectric permittivity and the Fermi velocity in graphite, respectively. Note, in order to approximate C_E, MLGNR is assumed to be a bundle of parallel ribbons displaced from a ground plane by the same distance, d [7]. Since the separation between any two subsequent layers is much smaller than d, the effect of the electrostatic capacitances between any two subsequent GNR layers is negligible. Furthermore, $L_K = R_Q/v_F = (125/NN_{ch})$ μH-cm^{-1} and $L_M \approx \mu d/WN$ represent the per unit length values of the kinetic and the magnetic inductances, in presence of the ground plane, wherein μ is the graphene permeability. In a practical case with $\mu \approx \mu_0 = 4\pi$ nH-cm^{-1}, d/W~1-10, and N_{ch}~1-10, the ratio of $L_M/L_K < 10^{-4}$ is ignorable.

In order to obtain the number of conducting channels in each GNR, one can add up contributions from all electrons in all n_C conduction sub-bands and all holes in all n_V valence sub-bands [10]:

$$N_{ch} = \sum_{i=1}^{n_C} \left[\exp\left((E_i - E_F)/kT\right) + 1\right]^{-1} + \sum_{i=1}^{n_C} \left[\exp\left((E_i - E_F)/kT\right) + 1\right]^{-1} \quad (1)$$

where i(=1, 2, 3, …) is a positive integer, E_F, k, T, and $E_i = ihv_F/2W$ are the Fermi energy, the Boltzmann constant, temperature, and the quantized energy of the i-th conduction or valence subband, respectively. This quantization is due to width confinement introduced by the ribbon′s finite width.

As illustrated in TLM equivalent circuit model of Fig. 1(b), MLGNR interconnect, is driven by a repeater of output resistance R_{out} and output parasitic capacitance C_{out}. It is driving an identical repeater with an input capacitance of $C_L = C_{out}$. In order to calculate the input-output transfer function for the configuration, shown in Fig. 1(b), one can use the ABCD transmission parameter matrix for a uniform RLC transmission line of length l as in [18].

$$T_{total} = \begin{bmatrix} A_T & B_T \\ C_T & D_T \end{bmatrix} \equiv \begin{bmatrix} 1 & R_{out} \\ 0 & 1 \end{bmatrix} \begin{bmatrix} 1 & 0 \\ sC_{out} & 1 \end{bmatrix} \begin{bmatrix} 1 & R_{ex} \\ 0 & 1 \end{bmatrix} \times \begin{bmatrix} \cosh(\gamma^T l) & Z_0^T \sinh(\gamma^T l) \\ Z_0^{-T} \sinh(\gamma^T l) & \cosh(\gamma^T l) \end{bmatrix} \begin{bmatrix} 1 & R_{ex} \\ 0 & 1 \end{bmatrix} \quad (2)$$

where $s=j\omega$ is the complex frequency, $R_{ex} = (R_C + R_Q)/2$, $Z_0^T = \sqrt{(R_S + sL)/(sC)}$ and $\gamma^T = \sqrt{(R_s + sL)sC}$. Elements of matrix T_{total} are given in Appendix A.

The input-output transfer function of the configuration in Fig. 1 can be written as:

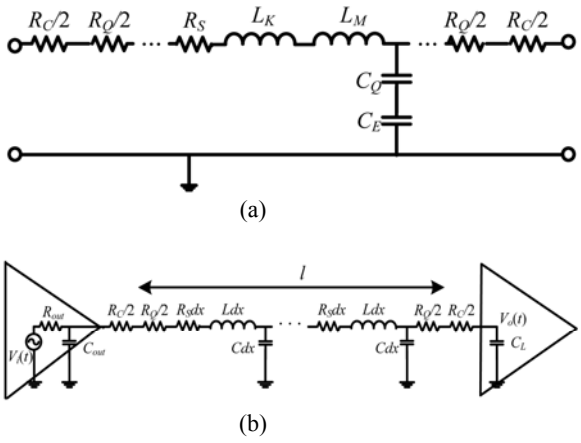

Fig. 1 Schematic of (a) a typical RLC model for MLGNR interconnects, and (b) a transmission line circuit model for a driver-MLGNR interconnect-load configuration [16].

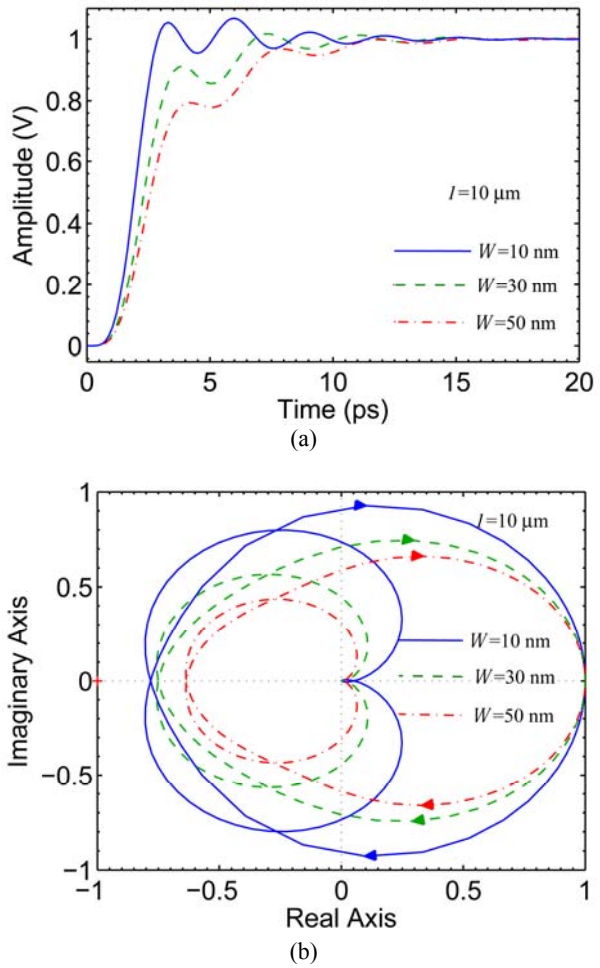

Fig. 2 Time domain responses (a) and Nyquist diagrams (b) calculated for driver-MLGNR interconnect-load configuration of Fig. 1, with R_{out}=100 Ω, C_L=C_{out}=1 fF, R_C=0, W=10 nm, and l=10, 30, and 50 μm.

$$H(s)=\frac{V_o(s)}{V_i(s)}=\frac{1}{A_T+sC_LB_T}\equiv \{\left[1+\left(R_{out}C_{out}+R_{out}C_L+2R_{ex}C_L\right)s+2R_{out}R_{ex}C_{out}C_Ls^2\right]\times \cosh\left(\gamma^T l\right)+\left[\left(R_{out}+R_{ex}\right)/Z_o^T+\left[\left(R_{out}R_{ex}C_{out}+R_{ex}\left(R_{out}+R_{ex}\right)C_L\right)/Z_0^T+Z_0^TC_L\right]s+\left(R_{out}R_{ex}^2C_{out}/Z_0^T+Z_0^TR_{out}C_{out}\right)C_Ls^2\right]\times\sinh\left(\gamma^T l\right)\}^{-1} \quad (3)$$

For simulation purposes, by expanding $\sinh(\gamma^T l)$ and $\cosh(\gamma^T l)$ in terms of Taylor series and keeping the appropriate terms, we can obtain a sixth order parametric linear approximation for (3).

$$H(s)\approx\left(\sum_{i=0}^{6}b_is^i\right)^{-1} \quad (4)$$

Coefficients b_i are given in Appendix B.

By varying the dimensions of interconnects (10 μm≤ l ≤50 μm and 10 nm≤W≤50 nm) and generating various step responses and Nyquist diagrams, we have studied the effect of MLGNR geometry on the step responses and relative stability of interconnects.

Using the fourth-order Padé's approximation, we have already studied the effects of MLGNR interconnect dimensions on its relative stability, when the contacts are perfectly ohmic (R_C = 0) [16]. Here, using a more accurate analysis (i.e., the sixth order linear approximation), by showing the Nyquist diagrams, we demonstrate the correspondence of interconnects relative stabilities with propagation delays, as nanoribbons' dimensions and contact resistance are varied.

3. Results and Discussion

According to (1) and assumption of metallic GNRs with E_F=0.1 eV, the number of conducting channels in each ribbon for W=10, 30, and 50 nm equals N_{ch}=2, 4, and 6, respectively. In this analysis, we have assumed C_{out}=C_L=1 fF, R_{out}=100 Ω, N=147 for MLGNR of thickness t≈50 nm (i.e., the separation between two adjacent GNRs δ~0.34 nm), and d=100 nm. The graphene permeability is also assumed to be μ=μ_0=4π nH-cm^{-1}.

By keeping MLGNR width constant and varying its length (l), we have realized that as l increases the propagation delay also increases. Note that as the length of the interconnect increases all of the resistances, inductances, and capacitances are increased. Therefore, delay of the interconnect increases. This, in turn, results in decrease in the amplitude overshoot. Figure 2 illustrates an example for the step responses (Fig. 2(a)) and Nyquist diagrams (Fig. 2(b)) for three interconnects of the same widths (W=10 nm), and lengths of l=10, 30, and 50 μm, with perfect ohmic contacts (i.e. R_C=0). As shown in Fig. 2(a), for l=10 μm (solid line) the propagation time is less than 2.5 ps (i.e. the time at which the step response reaches to 90% of its maximum), amplitude of the step response experiences an overshoot, and fluctuations are significant. Whereas, for l=30 μm (dashed line), the propagation delay has increased to ~17 ps, the overshoot has disappeared, and fluctuations has become less significant. For l=50 μm (dotted-dashed line) the propagation delay has increased further to values above 48 ps, and the fluctuations have disappeared. Figure 2(b) illustrate the corresponding Nyquist diagrams for interconnects of the given example, as for Fig. 2(a). As seen in this figure, the critical point (−1, 0) is outside the diagrams, for all three interconnects. To our expectation, as l increases, the Nyquist diagrams for l=30 and 50 μm move farther away from the critical point about 35% and 62% respectively. So the system's relative stability is increased. This behavior, in fact, is in accordance with that observed in Fig. 2(a).

Next, while keeping interconnect length constant, we have varied its width. We have observed that as W increases the propagation delay increases and the overshoot amplitude decreases. This is because, as W

increases C_E and N_{ch} both increase and L_M decreases. On the other hand, with an increase in N_{ch}, C_Q increases but R_Q, R_S, and L_K decrease. However, while C_E and C_Q have dominant role in determining the switching delay, role of R_Q, R_S, L_M, and L_K is insignificant. As an example, Fig. 3 illustrates the step responses (Fig. 3(a)) and Nyquist diagrams (Fig. 3(b)) of three interconnects of the same length (l=10 μm) and widths of W=10, 30, and 50 nm. Comparison of Fig 3(a) and Fig. 2(a) reveals that, interconnects step responses are less sensitive to the variations in ribbons widths than to the variations in their lengths. As observed in this comparison, when l is increased by a factor of three/five, the raise in propagation delay is ten times larger than that for the case in which W experiences the same relative increase. Propagation delays for W=30 and 50 nm are respectively equal to 5.3 and 6.7 ps. In accordance with the behavior observed in Fig. 3(a), Fig. 3(b) demonstrate that as W increases Nyquist diagrams move farther away from the critical point (−1, 0) that is outside all three. Nyquist diagrams for W=30 and 50 nm move farther away from critical point about 10% and 17% respectively. So the system's relative stability increases with W. Then, we examine the effect of contact resistance, R_C, on the step reposes and the relative stability of interconnects.

Figure 4 illustrates the results of this study, for three interconnects of the same lengths (l=10 μm) and widths (W=10 nm) and contact resistances of R_C=0, 1, and 10 kΩ. As shown in Fig. 4(a), the propagation delay increases significantly, as R_C increases from 0 (solid line) to 1 k Ω (dashed line) and then to 10k Ω (dotted-dashed line). The propagation delay for R_C= 1 and 10 kΩ equals to 9.7 ps and 77 ps respectively. In accordance with the behavior observed from this figure, Fig. 4(b) shows that corresponding Nyquist diagrams move farther away from the critical point (−1, 0) as R_C increases. For R_C= 1 and 10 kΩ the Nyquist diagrams move farther from critical point about 75% and 87% respectively. Hence, the system relative stability increases accordingly.

Figure 5 compares the results by the 4th and 6th order Pade's approximations for the MLGNR interconnect of l=10 μm, W=10 nm and R_C=0, that was shown to be the

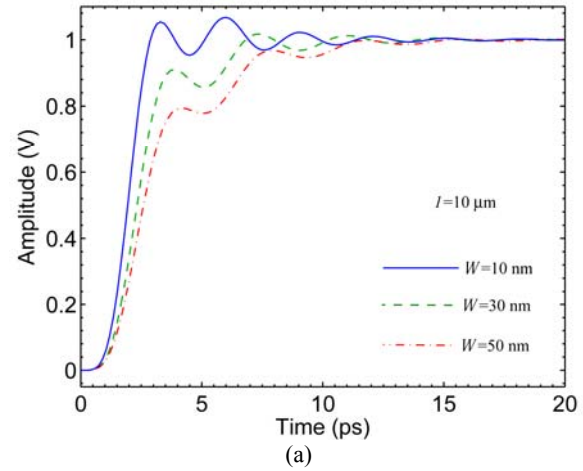

(a)

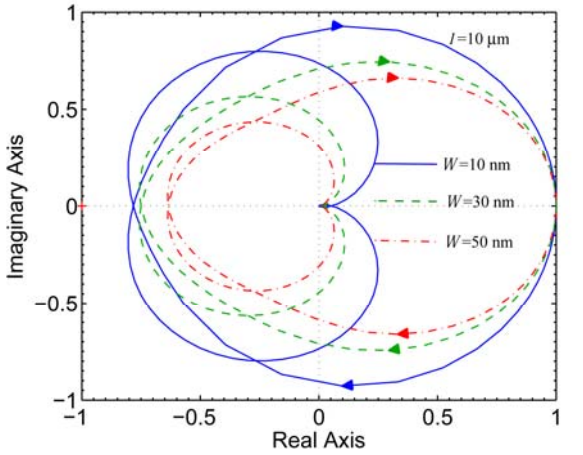

(b)

Fig. 3 Time domain responses (a) and Nyquist diagrams (b) calculated for driver-MLGNR interconnect-load configuration of Fig. 1, with R_{out}=100 Ω, C_L=C_{out}=1 fF, R_C=0, l=10 μm, and W=10, 30, and 50 nm.

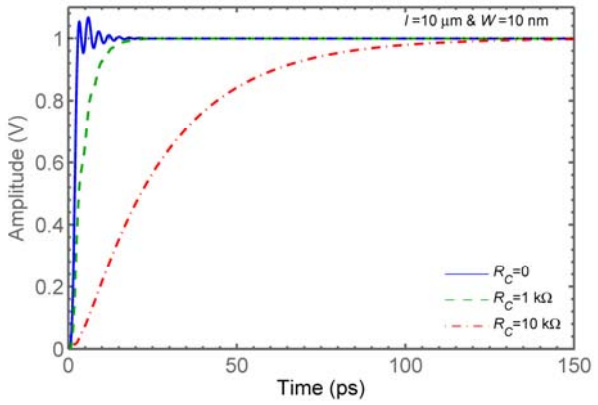

(a)

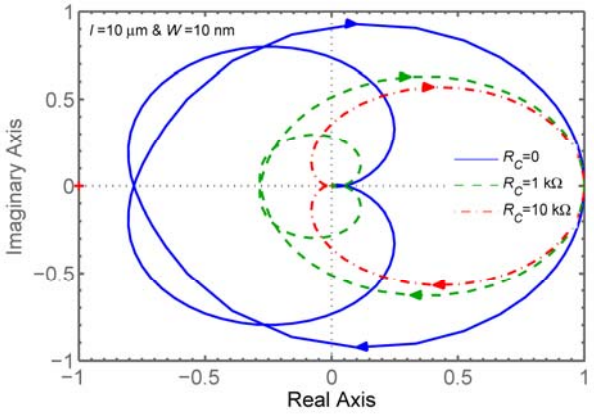

(b)

Fig. 4 Time domain responses (a) and Nyquist diagrams (b) calculated for driver-MLGNR interconnect-load configuration of Fig. 1, with W=10 nm, l=10 μm, R_{out}=100 Ω, C_L=C_{out}=1 fF, R_C=0, 1 kΩ, and10 kΩ.

worst case, as far as the stability is concerned, so far. The comparison shows that the peak overshoot of 1.087 V and the corresponding delay of 3.677 ps for the 4th order approximation are respectively about 23 mV higher and 2.145 ps shorter than the peak overshoot and delay obtained by the 6th order approximation. These correspond to a 26% overestimate for the peak overshoot and a 58% underestimate in the delay time. Furthermore, it reveals that the Nyquist diagram obtained by the 4th order is about 15% closer to critical point (-1, 0) compared to that obtained by the 6th order approximation.

Finally, we compare the step responses and Nyquist diagrams calculated for interconnects made of MLGNR and SWCNT bundle, considering all efficacious conditions to be same for both systems. Further assumptions made for this particular analysis are l=2 and 10 μm, W=t=50 nm, and SWNTs are identical with diameters of D=1 nm. For this diameter, the number of conduction channels in each SWNT, including the crystal and spin degeneracy, is N_{ch}=4. For the given dimensions, the number of SWCNTs in the bundle is N=1369. Figure 6 illustrates the results of this comparison.

As shown in Fig. 6(a), SWCNT bundle interconnects experience longer propagation delays and smaller fluctuations in their time responses, in comparison with their MLGNR rivals. In figure 6(a) propagation delay for MLGNR interconnects with l=2 and 10 μm equals 1.4 and 7.9 ps, respectively. Whereas, the propagation delay for SWCNT bundles with l=2 and 10 μm equals 19.9 and 99 ps, respectively. This is because, for SWCNT bundle interconnects, C_E and C_Q, which play the dominant role in determining the propagation delay, are larger than those of their MLGNR rivals are. Note, $C_{E\text{Bundle}} = \{2\pi\varepsilon/\log(d/D)\} \times \{W/(D+\delta)\} > C_{E\text{MLGNR}}$. On the other hand, the total number of conducting channels (i.e., NN_{ch}) in the given SWCNT bundle

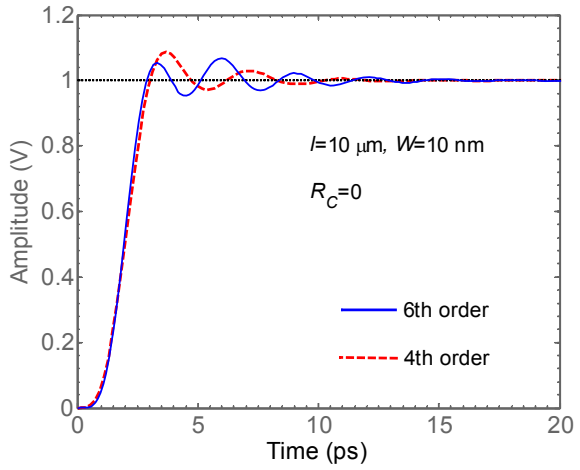

(a)

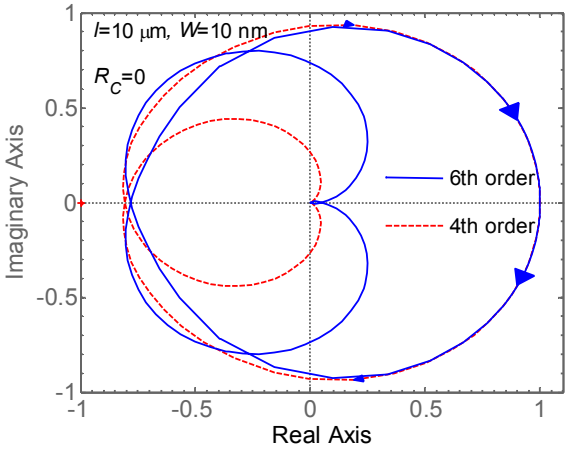

(b)

Fig. 5 Comparison of (a) Time domain responses and (b) Nyquist diagrams for driver-MLGNR interconnect-load configuration of Fig. 1, with W=10 nm, l=10 μm, R_{out}=100 Ω, C_L=C_{out}=1 fF, R_C=0, calculated by the 4th and the 6th order pade approximation.

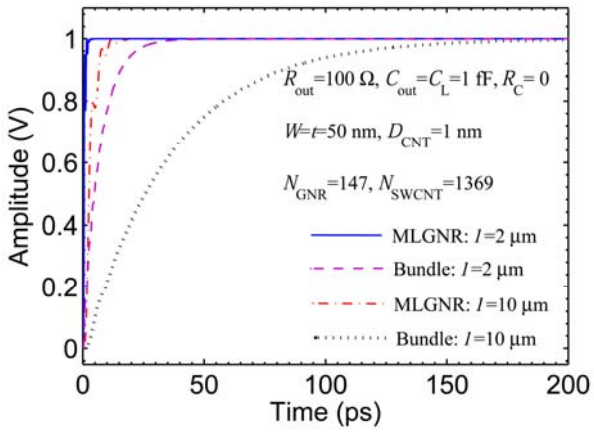

(a)

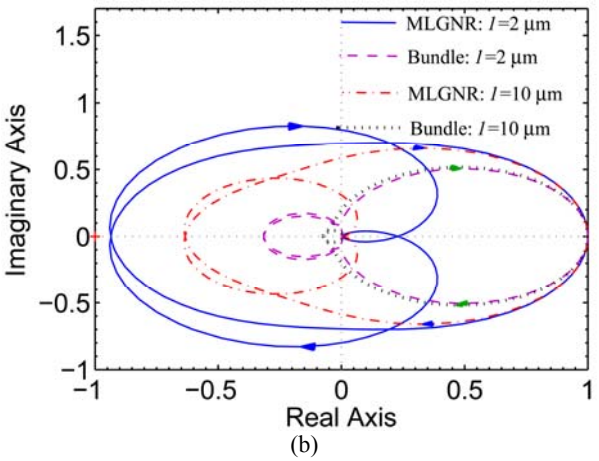

(b)

Fig. 6 Comparison of time domain responses (a) and the corresponding Nyquist diagrams (b) for MLGNR interconnects with those of their SWCNT bundle rivals, with l=2 and 10 μm, W=t=50 nm, D_{SWCNT}=1 nm, N_{GNR}=147, N_{SWCNT}=1369, R_{out}=100 Ω, and C_{out}=C_L= 1 fF, R_C=0.

interconnects (i.e., 2738) are more than three times larger than those for their MLGNR rivals (i.e., 882). As a result, for a SWCNT Bundle, C_Q is by the same factor larger than that for its MLGNR counterpart. Although R_Q, R_S, and L_K are all proportional to the inverse of NN_{ch}, their role in determining propagation delay is insignificant, as pointed out earlier.

The corresponding Nyquist diagrams shown in Fig. 6(b) demonstrates that interconnects made of SWCNT bundles are relatively more stable than those made of similar MLGNR. The Nyquist diagrams for SWCNT bundles with l=2 and 10 μm move about 0.66% and 88% further away from the critical point with respect to those of MLGNR interconnects of the same lengths, respectively. This behavior is in accordance with that observed from Fig. 6(a).

4. Conclusion

We have examined the dependence of multilayer graphene nanoribbon (MLGNR) interconnects on their dimensions and contact resistances. In doing so, we have used transmission line circuit modeling and linear parametric expression for the transfer function of a driver–MLGNR interconnect–load configuration. Using this formulation, which is a sixth order linear parametric approximate relation, we have simulated the step response of the cited configuration. Meanwhile, we have performed Nyquist stability analysis. Correlation between the step responses and their corresponding Nyquist diagrams are excellent. Simulations show that as MLGNRs′ lengths, widths, or contact resistances are increased, the propagation delays become longer and the systems become relatively more stable. We have also compared the time domain output responses and Nyquist diagrams of MLGNR interconnects with those of single wall carbon nanotube (SWCNT) bundle interconnects of the same external dimensions. Simulations show that propagation delays for SWCNT bundle interconnects are longer than those of their MLGNR counterparts. Hence, former interconnects are relatively more stable than latter interconnects. It was also shown that the 4th order approximation results in a considerable error with respect to the 6th order approximation. In order to reduce the error further, one needs to use a higher order approximation, in expense of more tedious mathematical relations and longer computational time. An alternative approach is to use a more exact matrix formulation which is under consideration by the authors.

References

[1] Noorden R. V., "Moving towards a graphene world," *Nature*, vol. 442, pp. 228–229, 2006.

[2] Novoselov K. S., Geim A. K., Morozov S. V., Jiang D., Zhang Y., Dubonos S. V., Grigorieva I. V. and Firsov A. A., "Electric field effect in atomically thin carbon films," *Science*, Vol. 306, No. 5696, pp. 666–669, 2004.

[3] Berger C., Song Z., Li X., Wu X., Brown N., Naud C., Mayou D., Li T., Hass J., Marchenkov A. N., Conrad E. H., First P. N. and Heer W. A. de, "Electronic confinement and coherence in patterned epitaxial graphene," *Science*, Vol. 312, pp. 1191-1196, 2006.

[4] Berger C., Song Z., Li T., Li X., Ogbazghi A. Y., Feng R., Dai Z., Marchenkov A. N., Conrad E. H., First P. N. and Heer W. A. de, "Ultrathin epitaxial graphite: 2D electron gas properties and a route toward graphene-based nanoelectronics," *J. Phys. Chem. B*, Vol. 108, pp. 19,912-19,916, 2004.

[5] Obradovic B., Kotlyar R., Heinz F., Matagne P., Rakshit T., Giles M. D., Stettler M. A. and Nikonov D. E., "Analysis of graphene nanoribbons as a channel material for field-effect transistors", *Appl. Phys. Lett.*, Vol. 88, pp. 142102-1, 2006.

[6] Nakada K., Fujita M., Dresselhaus G. and Dresselhaus M. S., "Edge state in graphene ribbons: Nanometer size effect and edge shape dependence", *Phys. Rev. B, Condens. Matter*, Vol. 54, pp. 17,954–17,961, 1996.

[7] Xu C., Li H. and Banerji K., "Modeling, analysis, and design of graphene nano-ribbon interconnects", *IEEE Transaction on Electron Devices*, Vol. 56, pp. 1567-1578, 2009.

[8] Shao Q., Liu G., Teweldebrhan D. and Balandin A. A., "High-temperature quenching of electrical resistance in graphene interconnects," *Appl. Phys. Lett.*, Vol. 92, pp. 2108-1, 2008.

[9] Zhu W., Perebeinos V., Freitag M. and Avouris P., "Carrier Scattering, Mobility, and Electrostatic Potential in Monolayer, Bilayer, and Trylayer Graphene", *Phys. Rev. B,* Vol. 80, pp. 235402-1, 2009.

[10] Naeemi A. and Meindl J., "Compact physics-based circuit models for graphene nanoribbon interconnects", *IEEE Transaction on Electron Devices*, Vol. 56, pp. 1822-1833, 2009.

[11] Naeemi A. and Meindl J. D., "Performance benchmarking for graphene nanoribbon, carbon nanotube, and Cu interconnects", in *Proc. Int. Interconnect Technol. Conf.*, pp. 183–185, Jun. 2008.

[12] Guo Z., Zhang D. and Gong X. G., "Thermal conductivity of graphene nanoribbon," *Applied Physics Letters*, Vol. 95, pp. 163103-1, 2009.

[13] Xu Y., Chen X., Gu B. L. and Duan W., "Intrinsic anisotropy of thermal conductance in graphene nanoribbons", *Applied Physics Letters*, Vol. 95, pp. 233116-1, 2009.

[14] Ouyang Y. and Guo J., "A theorical study on thermoelectric properties of graphene nanoribbons," *Applied Physics Letters*, Vol. 95, pp. 263107-1, 2009.

[15] Shen T., Gu J. J., Xu M., Wu Y. Q., Bolen M. L., Bolen M. A., Capano M. A., Engel L. W. and Ye P. D., "Observation of quantum- Hall effect in

gated epitaxial graphene grown on SiC (0001)", *Applied Physics Letters*, Vol. 95, pp.172105-1, 2009.

[16] Nasiri S. H., Moravvej-Farshi M. K. and Faez R., "Stability Analysis in Graphene Nanoribbon Interconnects", *IEEE Electron Device Lett*., Vol. 31, pp 1458-1460, 2010.

[17] Chen X., Lee K. J., Akinwande D., Close G. F., Yasuda S., Paul B., Fujita S., Kong J. and Wong H. P., "High-Speed Graphene Interconnects Monolithically Integrated with CMOS Ring Oscillators Operating at 1.3GHz", *IEDM 2009*, pp. 581-584, 2009.

[18] Fathi D. and Forouzandeh B., "Time domain analysis of carbon nanotube interconnects based on distributed RLC model," *Nano*, Vol. 4, No. 1, pp. 13–21, 2009.

APPENDIX A

With some mathematical manipulations Elements of matrix T in (2), become:

$$A_T = (1+sR_{\text{out}}C_{\text{out}})\cosh(\gamma^T l) + \frac{(R_{\text{out}}+2R_{ex}+2sR_{\text{out}}R_{ex}C_{\text{out}})}{Z_0^T}\sinh(\gamma^T l) \quad \text{(A1)}$$

$$B_T = [R_{\text{out}}+2R_{ex}+2sR_{\text{our}}R_{ex}C_{\text{out}}]\cosh(\gamma^T l) + \sinh(\gamma^T \ell)\times\left\{Z_0^T(1+sR_{\text{out}}C_{\text{out}}) + \left[R_{ex}(R_{\text{out}}+R_{ex}+sR_{\text{out}}R_{ex}C_{\text{out}}\right]/Z_0^T\right\} \quad \text{(A2)}$$

$$C_T = sC_{\text{out}}\cosh(\gamma^T l) + \frac{1+sR_{ex}C_{\text{out}}}{Z_0^T}\sinh(\gamma^T l) \quad \text{(A3)}$$

$$D_T = (1+2sR_{ex}C_{\text{out}})\cosh(\gamma^T l) + \left[sC_{\text{out}}Z_0^T + \frac{R_{ex}(1+sR_{ex}C_{\text{out}})}{Z_0^T}\right]\sinh(\gamma^T l) \quad \text{(A4)}$$

APPENDIX B

Coefficients b_i in (4) are b_0=1,

$$b_1 = R_{out}(C_{out}+Cl+C_L)+R_{ex}(Cl+2C_L)+R_S l\left(\frac{Cl}{2!}+C_L\right) \quad \text{(B1)}$$

$$b_2 = LlC_L + R_{ex}R_{out}(C_{out}Cl+C_LCl+2C_{out}C_L)+R_{ex}^2ClC_L + R_{out}R_S Cl^2\left(\frac{C_{out}Cl}{2!}+\frac{C^2l^2}{3!}+C_{out}C_L+\frac{ClC_L}{2!}\right) + R_{ex}R_S Cl^2\left(\frac{Cl}{3!}+C_L\right)+\frac{R_S^2C^2l^4}{4!}+\frac{LCl^2}{2!}+\frac{R_S^2Cl^3C_L}{3!} \quad \text{(B2)}$$

$$b_3 = \frac{2R_SLC^2l^4}{4!}+\frac{R_S^3C^3l^6}{6!} + \left(R_{ex}+R_{out}+\frac{R_S}{C}C_L\right)\times\left(\frac{LC^2l^3}{3!}+\frac{R_S^2C^3l^5}{5!}\right) + \left(R_{out}(C_{out}+C_L)+2R_{ex}C_L\right)\times\left(\frac{LCl^2}{2!}+\frac{R_S^2C^2l^4}{4!}\right) + \left(R_{ex}R_{out}(C_{out}+C_L)+R_{ex}^2C_L+\frac{LC_L+R_SR_{out}C_{out}C_L}{C}\right) \times\frac{R_SC^2l^3}{3!}+R_{ex}R_{out}C_{out}ClC_L(R_{ex}+R_Sl)+R_{out}C_{out}LlC_L \quad \text{(B3)}$$

$$b_4 = \frac{L^2C^2l^4}{4!}+\frac{3R_S^2LC^3l^6}{6!}+\frac{R_S^4C^4l^8}{8!} + \left[R_{\text{out}}(C_{\text{out}}+C_L)+2R_{ex}C_L\right]\times\left(\frac{2R_SLC^2l^4}{4!}+\frac{R_S^3C^3l^6}{6!}\right) + \left(R_{\text{out}}+R_{ex}+\frac{R_S}{C}C_L\right)\left(\frac{2R_SLC^3l^5}{5!}+\frac{R_S^3C^4l^7}{7!}\right) + 2R_{\text{out}}R_{ex}C_{out}C_L\left(\frac{LCl^2}{2!}+\frac{R_S^2C^2l^4}{4!}\right) + \left(R_{\text{out}}R_{ex}(C_{\text{out}}+C_L)+R_{ex}^2C_L+\frac{L}{C}C_L+\frac{R_S}{C}R_{\text{out}}C_{\text{out}}C_L\right) \times\left(\frac{LC^2l^3}{3!}+\frac{R_S^2C^3l^5}{5!}\right) + \frac{R_SC^2l^3}{3!}\left(R_{\text{out}}R_{ex}^2C_{\text{out}}C_L+\frac{L}{C}R_{\text{out}}C_{\text{out}}C_L\right) \quad \text{(B4)}$$

$$b_5 = [R_{out}(C_{out}+C_L)+2R_{ex}C_L] \times\left(\frac{L^2C^2l^4}{4!}+\frac{3R_S^2LC^3l^6}{6!}+\frac{R_S^4C^4l^8}{8!}\right) + 2R_{out}R_{ex}C_{out}C_L\times\left(\frac{2R_SLC^2l^4}{4!}+\frac{R_S^3C^3l^6}{6!}\right) + \left(R_{out}R_{ex}(C_{out}+C_L)+R_{ex}^2C_L+\frac{L}{C}C_L+\frac{R_S}{C}R_{out}C_{out}C_L\right) \times\left(\frac{2R_SLC^3l^5}{5!}+\frac{R_S^3C^4l^7}{7!}\right) + \left(R_{out}R_{ex}^2C_{out}C_L+\frac{L}{C}R_{out}C_{out}C_L\right) \times\left(\frac{LC^2l^3}{3!}+\frac{R_S^2C^3l^5}{5!}\right) \quad \text{(B5)}$$

Saeed Haji Nasiri was born in Tehran, Iran, in 1981. He received the B.S. and M.S. degrees in Electrical Engineering from the Qazvin Branch, Islamic Azad University, Qazvin, Iran, in 2004 and the Central Tehran Branch, Islamic Azad University, Tehran, Iran, in 2007, respectively. He is currently working toward the PhD degree at the Department of Electrical Engineering, Sciences and Research Branch, Islamic Azad University, Tehran, Iran. His research interests include Graphene nanoribbon (GNR) and carbon nanotube (CNT) interconnects.

Mohammad Kazem Moravvej-Farshi was born in Yazd, Iran, in 1952. He received the B.Sc. and the M.A. degrees in physics from Sharif University of Technology (SUT), Tehran, Iran, in 1976, and the University of Southern California (USC), Los Angeles, California, in 1978, respectively, the M.Sc. and the Ph.D degrees in electronics from the University of California at Santa Barbara (UCSB), in 1980, and the University of New South Wales (UNSW), Sydney, Australia, in 1987, respectively. From 1980 to 1984, he was a member of research staff with the Division of Microwave, Iran Telecommunication Research Center (ITRC). He joined Tarbiat Modares University (TMU) in 1987, where he is currently a Professor of Electronics. He has translated from English to Farsi four books in the field of semiconductor devices and one in laser electronics. His last translation in 2004 was selected as the best translation of the year in the field of engineering and applied sciences. M. K. Moravvej-Farshi was elected as one of the two most prominent professors of 2002 in the field of electrical engineering, nationwide.

Professor Moravvej Farshi is currently a senior member of IEEE and a senior member of the Optical Society of America (OSA). He is also one of the founders of the Optics and Photonics Society of Iran (OPSI).

Rahim Faez received B.S. degree from Sharif University of Technology in 1977 and the M.S. and Ph.D. degrees from UCLA in 1979 and 1985 respectively. Then he joined Sharif University of Technology and currently he is Associate professor in there. His research interests include design and simulation of advanced semiconductor nano and quantum devices.